Journal of Power Sources 256 (2014) 361–368

Contents lists available at ScienceDirect

Journal of Power Sources

journal homepage: www.elsevier.com/locate/jpowsour

Nitrogen-doped graphene/sulfur composite as cathode material for high capacity lithium–sulfur batteries

Xiwen Wang [a], Zhian Zhang [a,b,*], Yaohui Qu [a], Yanqing Lai [a,b], Jie Li [a,b,*]

[a] School of Metallurgy and Environment, Central South University, Changsha 410083, China
[b] Engineering Research Center of High Performance Battery Materials and Devices, Research Institute of Central South University in Shenzhen, Shenzhen 518057, China

HIGHLIGHTS

- Nitrogen-doped graphene sheets as a matrix to load sulfur for Li–S battery cathode.
- NGS/S cathode shows enhanced electrochemical properties compared with GS/S cathode.
- Pyridinic configuration contributes more to improved electrochemical performance.

GRAPHICAL ABSTRACT

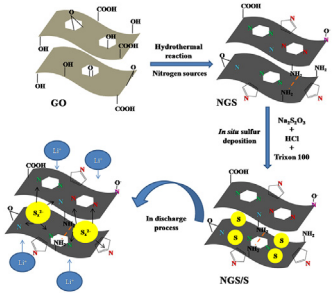

ARTICLE INFO

Article history:
Received 5 November 2013
Received in revised form
3 January 2014
Accepted 20 January 2014
Available online 28 January 2014

Keywords:
Nitrogen-doped graphene
Carbon–sulfur composites
Sulfur cathode
Lithium–sulfur battery

ABSTRACT

Two types of nitrogen-doped graphene sheets (NGS) synthesized by a facile hydrothermal method are used to immobilize sulfur via an *in situ* sulfur deposition route. The structure and composition of the prepared nitrogen doped graphene/sulfur (NGS/S) composites are confirmed with X-ray diffraction (XRD), X-ray photoelectron spectroscopy (XPS) and Raman spectroscopy. Scanning electron microscope (SEM) and Transmission electron microscope (TEM) images shows the porous sulfur particles are well wrapped by NGS. Compared with graphene/sulfur (GS/S) composite, the NGS-1/S composite with high loading (80 wt%) of sulfur presents a remarkably higher reversible capacity (1356.8 mAh g^{-1} at 0.1 C) and long cycle stability (578.5 mAh g^{-1} remaining at 1 C up to 500 cycles). Pyridinic-N rich NGS-1/S exhibits a better electrochemical performance than pyrrolic-N enriched NGS-2/S. The improvement of electrochemical properties could be attributed to the chemical interaction between the nitrogen functionalities on the surface of NGS and polysulfide as well as the enhanced electronic conductivity of the carbon matrix.

1. Introduction

Lithium–sulfur (Li–S) batteries have been recognized as one of promising high performance rechargeable lithium batteries due to the high specific capacity (1675 mAh g^{-1}), high energy density (2600 Wh kg^{-1}), low cost, and natural abundance of sulfur [1,2]. However, few commercial application have been realized because of the poor intrinsic conductivity of pristine sulfur resulting in low utilization and poor rate capacity of sulfur cathode, and the dissolution of polysulfide resulting in limited cycle stability and high self-discharge, and the large volume expansion/shrinkage of sulfur leading to severe pulverization of the electrode [2–5].

In recent years, many carbon materials have been reported as sulfur immobilizer to address these issues, such as mesoporous carbon [6–8], carbon nanotubes [9,10], hollow carbon

* Corresponding authors. Tel./fax: +86 731 88830649.
E-mail address: zza75@163.com (Z. Zhang).

0378-7753/$ – see front matter © 2014 Elsevier B.V. All rights reserved.
http://dx.doi.org/10.1016/j.jpowsour.2014.01.093

nanostructures [11,12] and graphene [13–19]. By encapsulating sulfur in carbon materials, the conductivity of cathode can be enhanced and the polysulfide dissolution into electrolyte can be inhibited to a certain extent. Among these materials, graphene sheets (GS) as a novel two-dimensional carbon materials with high electrical conductivity, large surface area, flexibility and chemical stability, exhibit great potential for the application in carbon–sulfur composites. The graphene sheets/sulfur (GS/S) hybrids for lithium sulfur batteries was synthesized by the mechanical mixing and following heat treatment, the specific capacity of which has increased from 800 to 1100 mAh g^{-1} at 50 mA g^{-1} [14]. The successive optimization of facile fabrication have been reported for different frameworks of GS/S composites including graphene wrapped sulfur particles [15–17], sandwich structured GS/S composite [18–20], sulfur/graphene hydrogel [21]. However, apart from the diverse textural characteristics, the properties of GS/S will also depend on the chemical interaction between functional groups on graphene and polysulfide. For example, the oxygen functional groups on graphite oxide (GO) [22] and the hydroxyl groups on hydroxylated graphene [23] were both found to be beneficial for the binding of polysulfide to C–C bonds owing to induced ripple by the functional groups, and in turn, high reversibility and stable cycling performance could be obtained.

Nitrogen doped graphene (NGS) is the most attractive heteroatom doped graphene and has been extensively investigated in the field of energy storage systems, such as lithium ion battery, supercapacitor and lithium–air battery [24–26]. Meanwhile, nitrogen doping also has been proven to be an effective strategy to improve overall electrochemical performance of the carbon host for Li–S batteries. Sun et al. reported the N-doped mesoporous carbon/sulfur composites, which presented the higher discharge potential and higher initial capacity of 1420 mAh g^{-1} compared to activated carbon. But the nitrogen content of N-doped mesoporous carbon (3.3 wt%) and the sulfur content of these composites (24 wt%) are still low [27]. Long et al. prepared N-doped mesoporous carbon with controllable nitrogen content by a facile colloid silica nanocasting. With the optimized nitrogen content of N-doped carbon (8.1 wt%) and the higher sulfur loading (60 wt%), the composites delivered a high reversible discharge capacity of 758 mAh g^{-1} at 0.2 C and 620 mAh g^{-1} at 1 C after 100 cycles [28]. A latest report about the first-principle study on the N-doped carbon nanotubes as cathode for Li–S batteries also predicted its huge potential [29]. Therefore, by NGS/S composite with proper nitrogen doping level will be a novel and promising cathode material for Li–S batteries.

In this work, N-doped graphene was applied in cathode materials of lithium sulfur battery for the first time. Two types of NGS were fabricated by a simple and low-cost one-pot hydrothermal method as illustrated in Fig. 1. Nitrogen doping and reduction of GO were finished simultaneously. Subsequently, the sulfur particles were deposited onto the N-doped graphene sheets through an *in situ* precipitation process with a high sulfur loading of 80 wt%. Physical characteristic and electrochemical performance of GS/S and NGS/S composites were investigated in details. Furthermore, we discuss the effect of distribution of nitrogen bonding configurations on electrochemical performance of NGS/S composite electrode.

2. Experiment

2.1. Preparation of N-doped graphene sheets

GO was prepared by a modified Hummers method in which natural graphite flakes were oxidized by a mixture of $NaNO_3$, $KMnO_4$ and concentrated H_2SO_4 as described previously [30].

To fabricate NGS, 40 mg GO was well dispersed in 40 mL deionized water by ultrasonic agitation for 2 h. Then, 1 mL ethylenediamine or 8 g urea was added into GO aqueous solution under vigorous stirring for 10 min, and the solution was transferred into a 60 mL Teflon-lined stainless steel autoclave. The autoclave was sealed and heat-treated at 180 °C for 12 h. After cooling, the solids at the bottom were filtered and washed for several times with deionized water until pH reached 7.0. the As-prepared samples using ethylenediamine and urea were denoted as NGS-1 and NGS-2 respectively. Finally, the collected products were freeze-dried under vacuum at 0 °C. For comparison, GS were synthesized through the above steps without the addition of nitrogen sources.

2.2. Preparation of N-doped graphene sheets/sulfur composite

The NGS/S composites were prepared following an *in situ* sulfur deposition strategy. Typically, 0.02 mol $Na_2S_2O_3$ and 0.5 mL Trixon-100 were dissolved in 500 mL deionized water by stirring. Then, 0.075 g as-prepared NGS or GS was suspended in the solution under sonication for 30 min. To precipitate sulfur onto surface and interspaces of NGS, 35 mL concentrated HCl (0.5 M) was slowly dropped into the solution and the reaction processed at room temperature for 6 h with magnetic stirring. The collected sample was filtered, washed with deionized water and ethanol, and dried in vacuum at 50 °C.

2.3. Structural characterizations

The surface morphology was characterized by scanning electron microscope (SEM, Nova NanoSEM 230), transmission electron microscope (TEM, Tecnai G2 20ST). Crystal structural characterization was carried out with X-Ray diffractometer (XRD, Rigaku D/max 2550VB$^+$) from 10° to 80° with Cu Kα radiation. Thermogravimetric analysis (TGA, SDTQ600) was conducted in determining the sulfur content in the composites under a nitrogen atmosphere. Surface functional groups and bonding characterization were performed by using X-ray photoelectron spectroscopy (XPS, Thermo Fisher ESCALAB250xi). The XPS curve fittings were performed using the

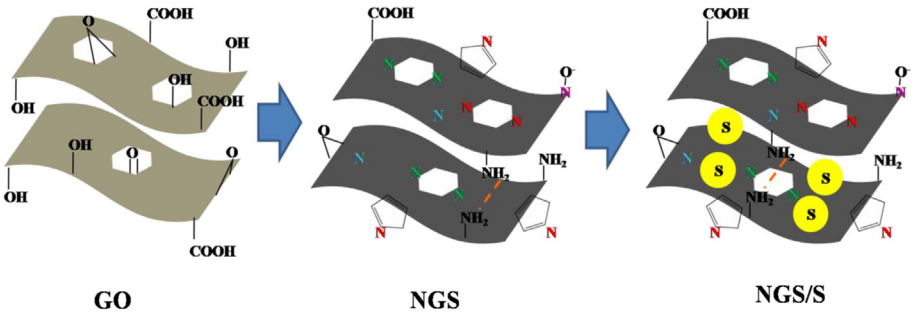

Fig. 1. Schematic representations of the synthesis process of NGS/S composites.

XPS Peak 41 program with Gaussian–Lorentzian functions after subtraction of a Shirley background. The fitting errors of XPS test results using this method are within ±1%. Raman spectra were tested with Dior LABRAM-1B instrument.

2.4. Electrochemical measurements

The electrochemical characterization was performed using a CR-2025 type coin cell. The cathode was prepared by mixing NGS/S composites or GS/S composites (80 wt%), acetylene black (10 wt%) and polyvinylidene fluoride (PVDF) binder (10 wt%) in an *N*-methyl pyrrolidinone (NMP) solvent. Then, the slurry was uniformly spread onto aluminum foil (20 μm), and dried at 60 °C under vacuum overnight. Test cells consisting of a lithium metal anode, a Celgard 2400 separator and the cathode were assembled in an argon-filled glove box (Universal 2440/750). 1 M bis (trifluoromethane) sulfonamide lithium salt (LiTFSI, Sigma Aldrich) and 0.1 M $LiNO_3$ in a mixture of 1,3-dioxolane (DOL) and 1,2-dimethoxyethane (DME) with a volume ratio of 1:1 was used as the electrolyte.

Cycle voltammetry (CV) test and electrochemical impedance spectroscopy (EIS) measurement were conducted with PARSTAT 2273 electrochemical measurement system. The CV tests were performed at a scan rate of 0.1 mV s^{-1} in the voltage range of 1.5–3.0 V. The EIS were measured in the frequency range from 100 kHz to 0.1 Hz with AC voltage amplitude of 5 mV at open-circuit voltage. The galvanostatic charge/discharge tests were carried out in potential range from 1.5 to 3.0 V with a LAND CT2001A battery-testing system. The cells were first discharged to 1.5 V and then the cycle number was counted. All the electrochemical tests were conducted at room temperature.

3. Results and discussion

3.1. Structure and morphology characterizations

In order to confirm the chemical composition and surface properties of different graphene sheets and graphene/sulfur composites, XPS measurements were performed and the results are exhibited in Fig. 2. The survey spectra in Fig. 2a prove the existence of N1s peak in NGS and co-existence of N1s, S2p and S2s peaks in NGS/S composites, indicating the successful nitrogen doping into GS and incorporation of sulfur in NGS/S composites. The peaks centered at about 285.0 eV and 531.0 eV in all survey

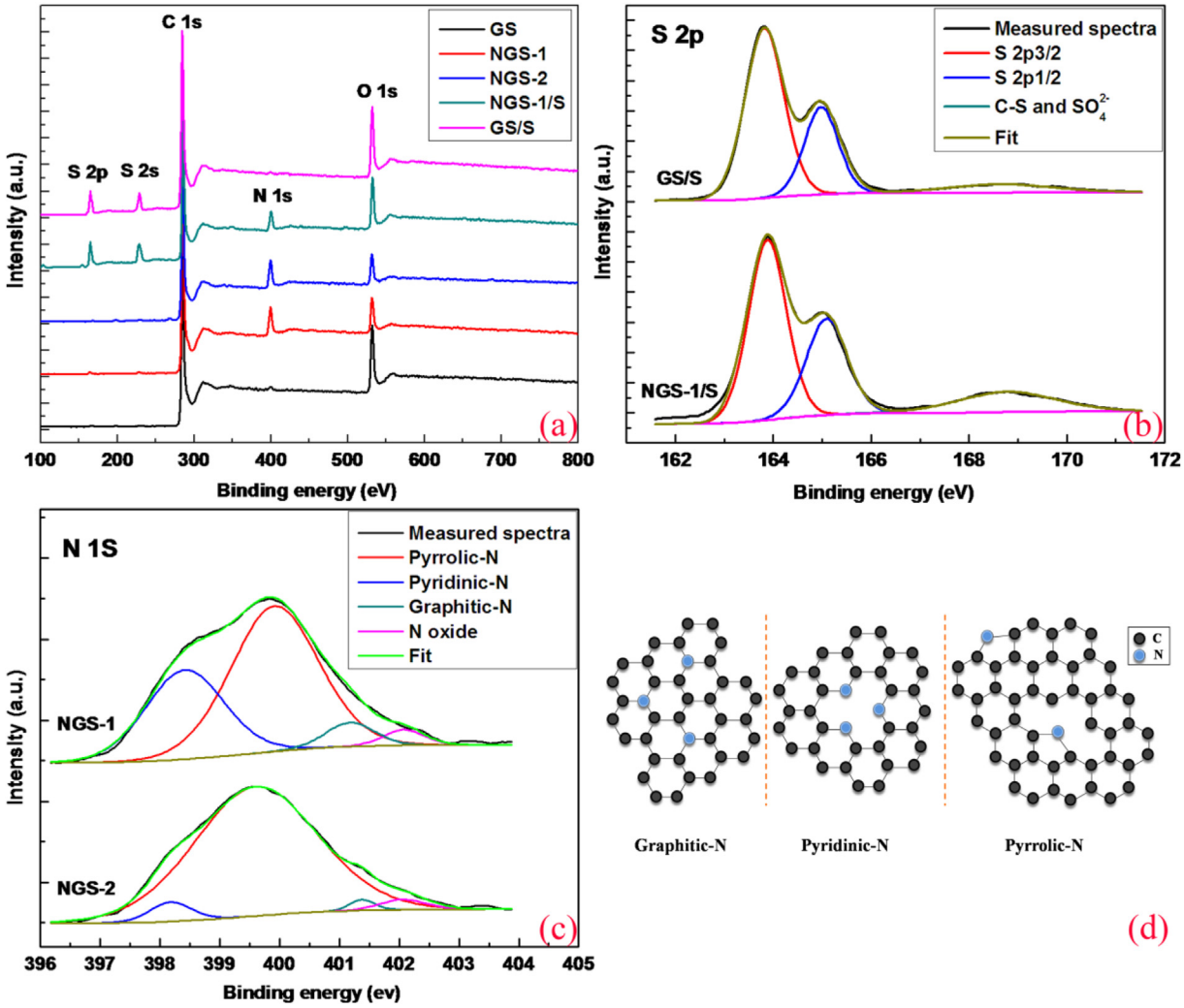

Fig. 2. (a) XPS survey spectra of GS, NGS, GS/S and NGS-1/S; (b) high-resolution S2p XPS spectrum of GS/S and NGS-1/S composites; (c) high-resolution N1s XPS spectrum of different NGS samples; (d) schematic model of three types of N-doped graphene: graphitic, pyridinic, pyrrolic.

spectra corresponds to the C1s and O1s, respectively. Fig. 2b displays the S2p spectra for GS/S and NGS-1/S composites. The $S2p_{1/2}$ peak at 163.7 eV and $S2p_{3/2}$ peak at 164.9 eV with an intensity ratio of 1:2 are the characteristic of solid sulfur in composite [31]. Another weak broad peak located between 168 and 170 eV can be attributed to the surface oxidation of sulfur or interaction between sulfur and graphene [32]. The percentage of nitrogen doping and distribution of nitrogen species in NGS are also given in Table. 1. As estimated by XPS results, the atom percent of nitrogen are 12.5 at% for NGS-1 and 11.5 at% for NGS-2. The high resolution N1s peaks (Fig. 2c) can be divided into four components including pyridinic-N (398.4 eV), pyrrolic-N (400 eV), graphitic-N (401.2 eV) and pyridine-N-oxide (402.3 eV) [33]. Both for NGS-1 and NGS-2, the pyrrolic-N predominates. However, for NGS-1 the ratio of the pyridinic-N to overall nitrogen is obviously higher than NGS-2. The difference in distribution of nitrogen bonding configurations may influence the electrochemical properties of NGS/S composites.

To further compare the structural and compositional properties of NGS/S and GS/S composites, XRD, Raman and TGA were carried out, as shown in Fig. 3. The XRD patterns of NGS/S and GS/S composites (Fig. 3a) can be well indexed by the orthorhombic sulfur crystalline (JCPDS 08-0247), proving that *in situ* precipitation route is an efficient way to prepare high-purity sulfur composites. The broad peaks of graphene are undetectable due to the high content of sulfur in composite. Raman spectroscopy is presented in Fig. 3b. Two sharp peaks of NGS/S below 600 cm^{-1} can be assigned to the S–S bond in composites [17]. Typical peaks of graphene-based materials are D band around 1340 cm^{-1}, G band around 1590 cm^{-1} as well as very weak 2D band at 2700 cm^{-1}. In general, the intensity ratio of D and G peak (I_D/I_G) reflects the disorder density of carbon materials. As revealed in inset in Fig. 3b, compared with GO (0.94), the I_D/I_G of GS is increased to 1.10 due to the unrepaired defects after the removal of oxygen-containing functional groups. However, the higher I_D/I_G of NGS (1.24) indicates more defects generate in sp^2 network during nitrogen doping. After *in situ* sulfur deposition, the I_D/I_G of NGS falls to 1.05, which demonstrates that the reaction of sulfur with nitride groups and oxygenated groups in NGS can decrease the disorder degree of NGS [34] The sulfur content of NGS/S and GS/S composites were determined by thermogravimetric analysis (Fig. 3c). The loading of sulfur in NGS-1/S, NGS-2/S and GS/S composites is estimated to 79.9, 80.0 and 83.2 wt%, respectively. High sulfur content in composites will ensure the high overall energy density per gram of cathode in Li–S batteries.

The morphology and microstructure of NGS-1/S and GS/S composites were investigated by SEM and TEM. In contrast to the GS/S composite, the NGS-1 composite possesses the sulfur particles with a smaller size of 0.5 μm as well as the rough and crumpled surface of graphene (Fig. 4a and b). Elemental X-ray mapping (Fig. 4c–e) presents a homogeneous distribution of sulfur, nitrogen and carbon in NGS-1/S composite. TEM images (Fig. 5) further provide structural information of NGS-1/S composite. Fig. 5a also illustrates that the sulfur microstructures in size of 0.5 μm are well anchored onto the N-doped graphene. The sulfur microstructures consist of sulfur nanoparticles in diameter of 20–50 nm (Fig. 5b).

Table 1
Carbon, nitrogen, oxygen content and N distribution of NGS from XPS measurement.

	C at%	N at %	O at%	Pyridinic-N at%	Pyrrolic-N at%	Graphitic-N at%	Pyridine-oxide at%
NGS-1	80.2	12.5	7.3	32.6	59.0	5.4	3.0
NGS-2	80.7	11.5	7.8	4.7	90.7	1.6	2.0

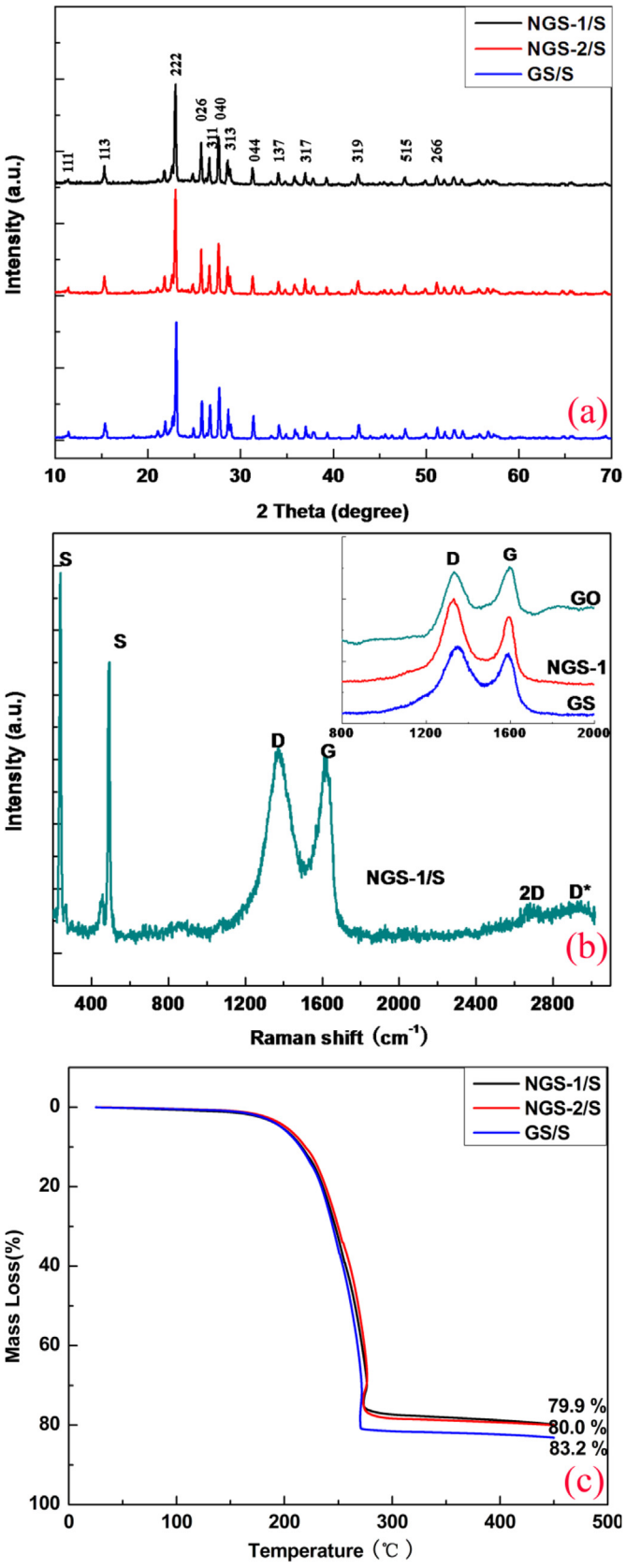

Fig. 3. (a) XRD patterns of GS/S and NGS/S composites; (b) Raman spectra of NGS-1/S composites; (c) TGA curves of the GS/S and NGS/S composites in nitrogen atmosphere. Inset (b) shows the Raman spectra of GO, GS and NGS.

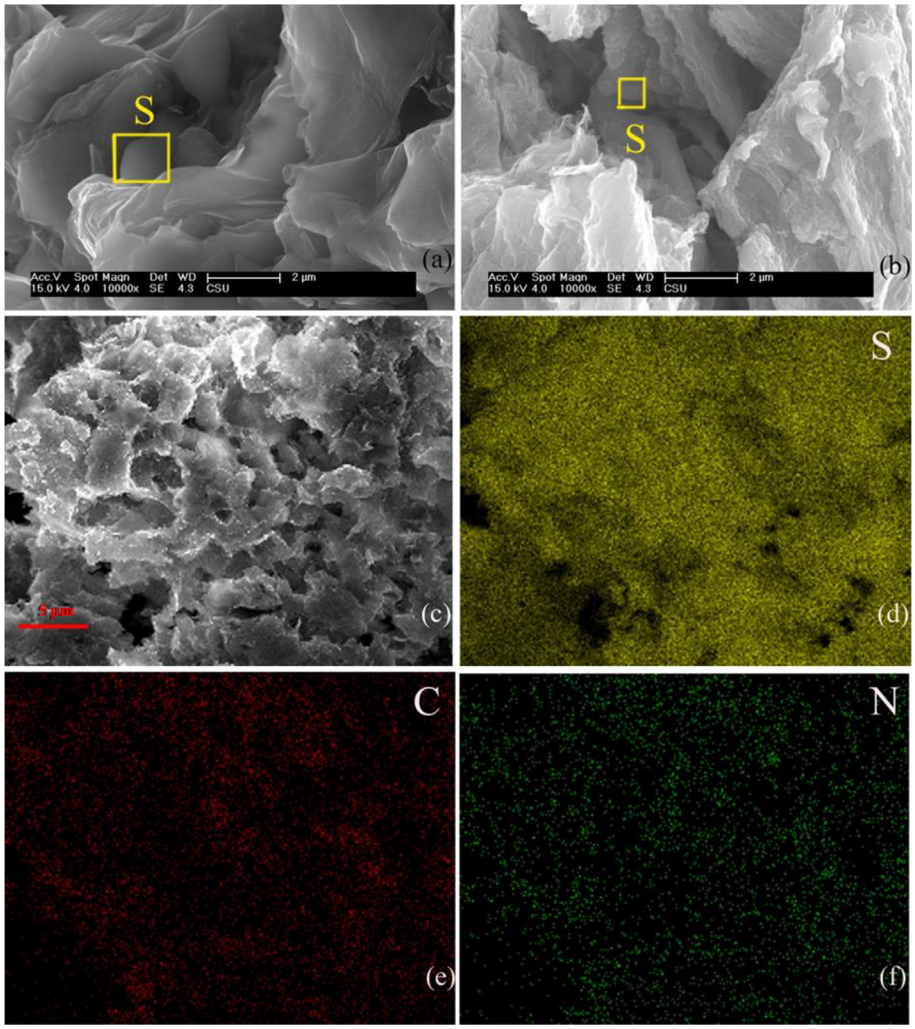

Fig. 4. FESEM images of (a) NGS-1/S and (b) GS/S composites; (c)–(f) SEM image and elemental X-ray mapping of NGS-1/S hybrid materials.

3.2. Electrochemical properties of NGS/S composite cathode materials

The electrochemical performance of NGS/S and GS/S composites cathode was tested by CV, EIS and galvanostatic charge/discharge measurements. Fig. 6a shows the CV profiles of NGS-1/S cathode between 1.5 and 3 V vs. Li^+/Li for initial three cycles at a scan rate of 0.2 mV s^{-1}. The sharp redox peaks with stable overlapping features confirm the high reversibility and excellent stability of electrode [21,23]. In the cathodic reduction process, the peak at 2.32 and 2.03 V can be assigned to the reduction of element sulfur (S_8) to soluble lithium polysulfides (Li_2S_n, $4 \leq n \leq 8$) and further

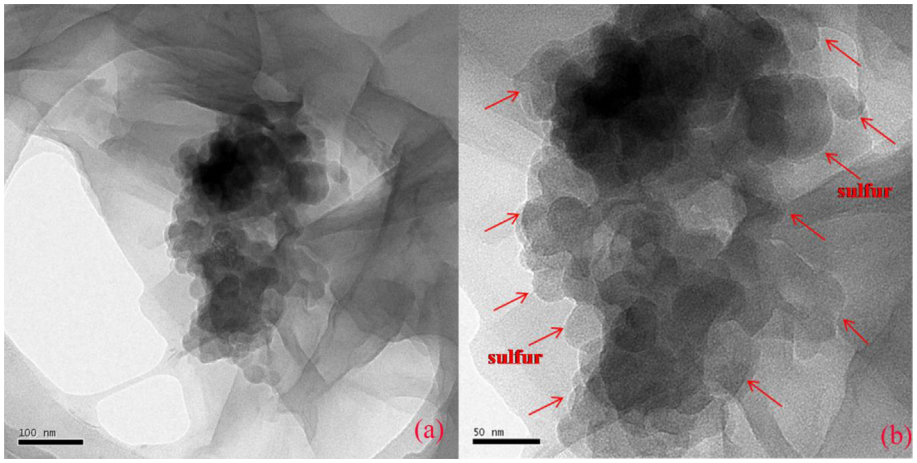

Fig. 5. TEM images of NGS-1/S composites.

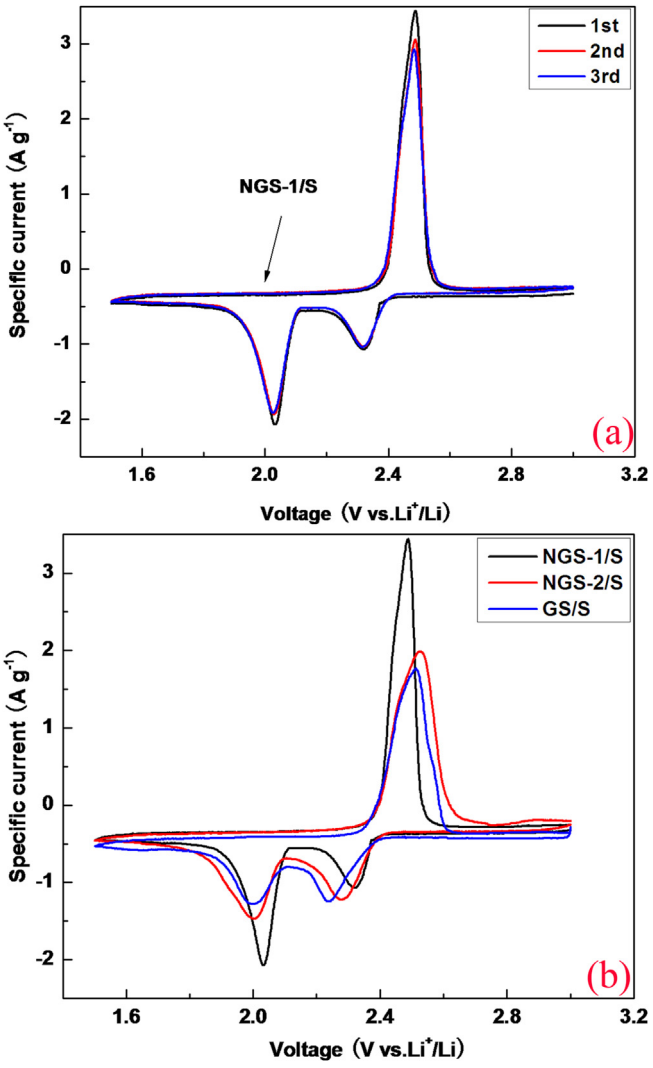

Fig. 6. (a) Cycle voltammetry plots of NGS-1/S electrode at a scan rate of 0.2 mV s^{-1} for the initial three cycles; (b) CV plots of GS/S, NGS-1/S and NGS-2/S electrodes at 0.2 mV s^{-1} for the first cycle.

conversion of these lithium polysulfides to insoluble Li_2S_2 and Li_2S, respectively [35]. The only anodic peak at 2.49 V corresponds to the transformation of Li_2S_2 and Li_2S to Li_2S_8 [23]. As revealed in Fig. 6b, the potential difference between cathodic and anodic peaks of NGS-2/S and GS/S cathodes was slightly increased, indicating the relatively large polarization of the electrodes. Moreover, apart from the redox peaks of sulfur, no other peaks can be observed, which suggests that nitrogen atoms in NGS will not participate in the reduction/oxidation process of sulfur [28].

Fig. 7a and b displays the charge–discharge curves of NGS-1/S and GS/S cathodes at 0.1 C, respectively. It can be obviously observed that the two discharge potential plateaus are consistent with two cathodic peaks in CV curves. The prolonged plateau around 2.0 V contributes to the main discharge capacity. The overcharging capacity of NGS-1/S cathode is less than 100 mAh g^{-1}, implying that the nitrogen doping minimize the shuttle phenomenon [8]. In addition, the potential plateaus of NGS-1/S cathode are still stable and distinct after 50 cycles, which indicate the excellent electrochemical performance of NGS-1/S composites [21].

The cycling performance of NGS/S and GS/S composites cathodes at 0.1 C were shown in Fig. 8a. The capacity is calculated based on the mass of sulfur. Without the nitrogen doping, the GS/S cathode delivers a considerable discharge capacity of 1272.4 mAh g^{-1} for the first cycle at 0.1 C, but which rapidly decreases to 582.4 mAh g^{-1} after 100 cycles. In contrast, the NGS-1/S and NGS-2 cathodes exhibit the slightly higher initial capacity of 1356.8 and 1298.6 mAh g^{-1} at 0.1 C, respectively. After 100 cycles, the NGS-1/S and NGS-2/S cathode maintain the specific capacity of 847.4 and 764.8 mAh g^{-1} with corresponding Columbic efficiency of 97.7 and 100.7%. In addition, a long-term discharge–charge test at 1 C for 500 cycles was performed for NGS-1/S cathode (Fig. 9). The specific capacity of this cathode stabilizes around 660.0 mAh g^{-1} after 100 cycles and achieves 578.5 mAh g^{-1} after 500 cycles, and its Columbic efficiency almost reaches 100% for each cycle. Therefore, the nitrogen doping effectively improves the cycling stability of graphene/sulfur composite cathode. Meanwhile, the better performance of NGS-1/S composites than NGS-2/S composites could be attributed to the stronger absorption ability to polysulfide species for NGS with a higher content of pyridinic-N. Based on the schematic model of nitrogen binding configurations in Fig. 2d, the pyridinic-N substitutes the carbon atom on C_6 ring at the edge of graphite layer and contributes one pair of lone electrons. Because of the strong inter-atomic interaction between pyridinic-N and polysulfide species, the polysulfide will be trapped in the carbon matrix. The pyrrolic-N is a nitrogen atom on the five-membered ring and contributes two p-electrons to π systems, thus the absorption ability of pyrrolic-N atom is weaker than that of

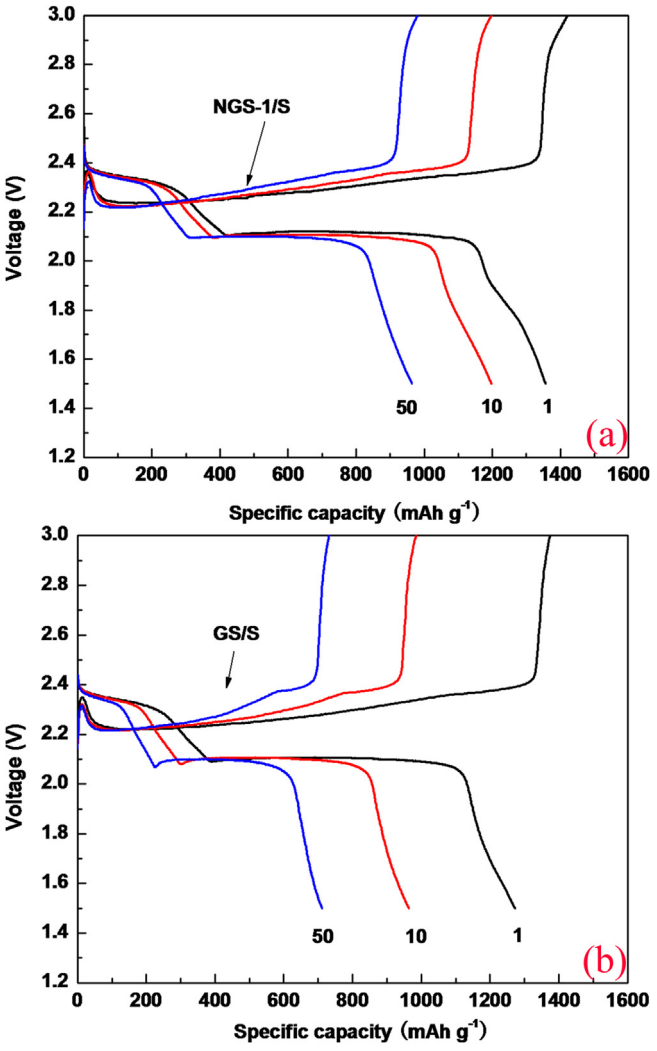

Fig. 7. Charge–discharge profiles of (a) NGS-1/S and (b) GS/S electrodes at 0.2 C.

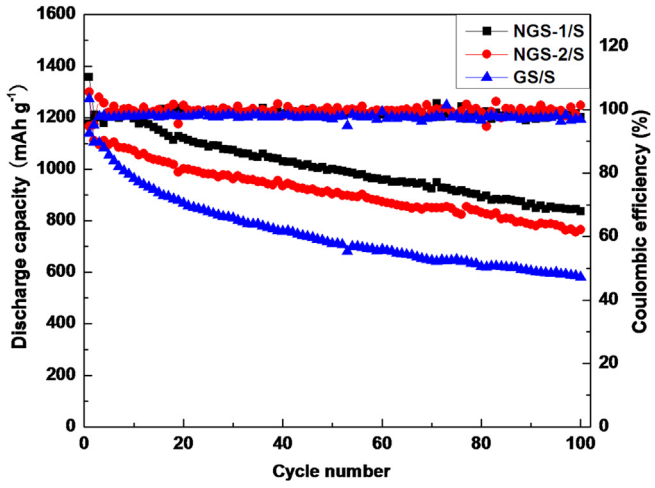

Fig. 8. Cycle performance of GS/S and NGS/S electrodes at 0.1 C; Inset shows the corresponding Coulombic efficiency.

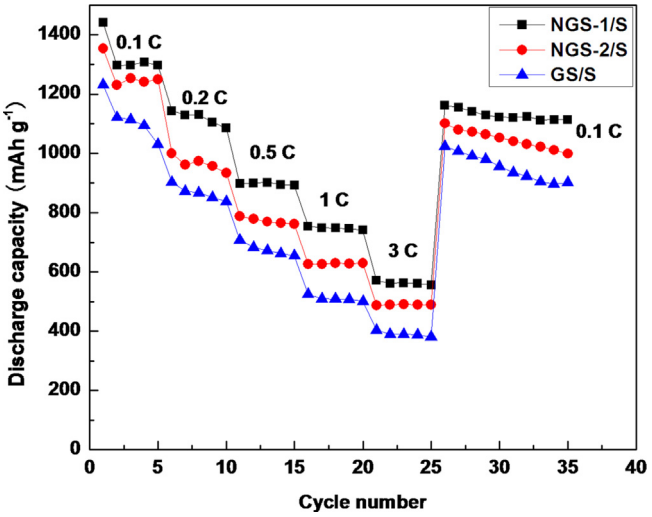

Fig. 10. Comparison of rate capability of GS/S, NGS/S electrodes at rates from 0.1 C to 3 C.

pyridinic-N [28]. The graphite-N structure is obtained by employing the N atom to substitute the carbon atom inside graphite plane, which is regarded as electron acceptor due to the higher electronegativity of nitrogen (3.04) than carbon (2.55). The pyridine-N-oxide is the pyridinic nitrogen atom bonds to oxygen functional groups [36]. Thus, increasing the proportion of pyridinic-N in NGS will be beneficial to the more effective surface absorption to polysulfide species and subsequently improve the overall electrochemical performance of NGS/S composite.

Except for the long cycling life, rate capability of NGS/S and GS/S composites at different rates were also performed, as present in Fig. 10. With the gradually increasing rates, the discharge capacity of NGS-1/S cathode decreases more slowly than the NGS-2/S and GS/S cathode at same rate. It is noted that the NGS-1/S cathode presents a steady reversible capacity of 562.0 mAh g^{-1} at 3 C, which is higher than that of GS/S cathode at 1 C. When the current rate returns back to 0.1 C, the capacity of NGS-1/S cathode recovers to 1140.0 mAh g^{-1}, indicating a stable structure of NGS-1/S cathode to tolerate the abuse of Li–S cells under various current densities.

To further understand the effect of nitrogen doping in graphene for improved rate performance of NGS/S composites, EIS measurements of NGS/S and GS/S fresh electrodes were carried out and collected in Fig. 11. The Nyquist impedance plots of three electrodes exhibit a semicircle at high frequency and a straight line at low frequency. The R_e refers to the resistance of electrolyte. The semicircle corresponds to a parallel element, the charge-transfer resistance (R_{ct}) and the constant phase capacitance (*CPE*) [37]. It is apparently that NGS/S cathodes exhibit a much lower charge-transfer resistance (30.6 Ω for NGS-1/S and 39.2 Ω for NGS-2/S) than GS/S cathode (88.9 Ω). Meanwhile, the straight line in low frequency represents the Warburg resistance (*W*), which is a measure of the ion diffusion in cathode. The steep slope of three cathodes suggests the fast diffusion of ions in porous sulfur electrode during charge/discharge process. In good agreement with EIS results, the electrical conductivity of GS/S and NGS-1/S composites, measured by a four-contact method, are estimated to be 2.3 and 1.5 S cm^{-1}, respectively. These date further confirm that the nitrogen doping boost the conductivity of graphene framework.

On account of the results above, the remarkable enhancement in cycling performance of NGS/S cathodes may be ascribed to four aspects: (1) nitrogen doping improve the electronic conductivity of graphene framework; (2) interaction between the nitrogen atoms and soluble polysulfides results in the reduced mass loss of sulfur and suppressed shuttle phenomenon; (3) the graphene nanosheets provide a large surface for well-anchored sulfur microstructure and accommodate the volume charge, which will stabilize the structure of electrode; (4) the porosity of sulfur microstructure as well as channel between graphene and sulfur particles facilitate ion transportation.

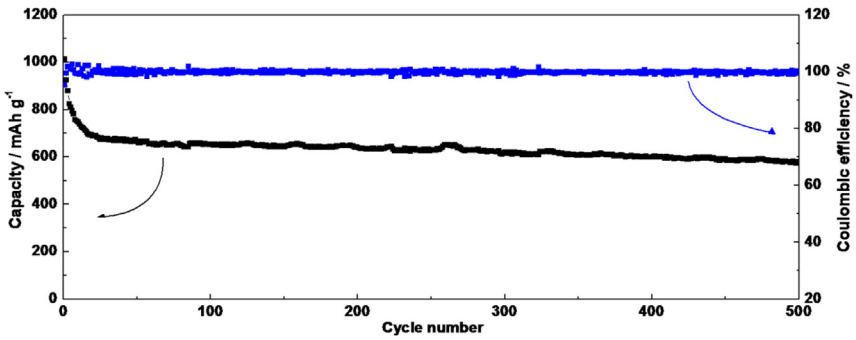

Fig. 9. Long-term performance of NGS-1/S electrode for 500 cycles at 1 C.

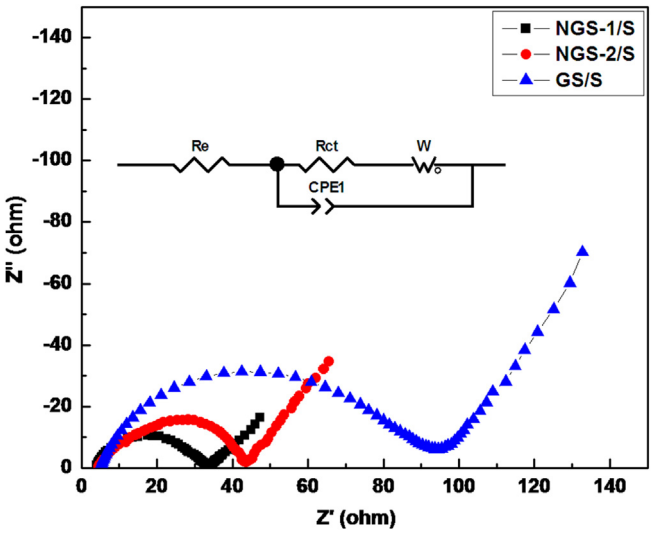

Fig. 11. EIS spectra of GS/S and NGS/S fresh electrodes at open-circuit potential.

4. Conclusion

In summary, NGS were prepared by a hydrothermal method and then the NGS/S composites were synthesized by an *in situ* deposition of sulfur onto NGS. The nitrogen doping could not only improve the electronic conductivity of graphene framework but also assist the graphene to immobilize sulfur and confine the diffusion of soluble polysulfides. The graphene frameworks also can buffer the volume change of electrode in charge/discharge process. As a result, the NGS-1/S composites with high sulfur loading of 80 wt% exhibits well reversibility, excellent cycling stability of 578.5 mAh g^{-1} after 500 cycles at 1 C and remains high specific capacity of 562.0 mAh g^{-1} at 3 C. Additionally, the pyridinic configuration has been proven to be the more important contribution to the enhanced electrochemical performance. These exciting results provide a promising candidate of cathode materials for Li–S batteries and a rational direction for designing cathode materials by using the advanced heteroatom doped graphene beyond NGS.

Acknowledgments

The authors acknowledge Dr. Haiyan Wang and Financial support by the Teacher Research Fund of Central South University (2013JSJJ027), the Fundamental Research Funds for the Central Universities of Central South University (No. 2013zzts026) and the Strategic Emerging Industries Program of Shenzhen, China (JCYJ20120618164543322).

References

[1] P.G. Bruce, S.A. Freunberger, L.J. Hardwick, J.M. Tarascon, Nat. Mater. 11 (2012) 19–29.
[2] X.L. Ji, L.F. Nazar, J. Mater. Chem. 20 (2010) 9821–9826.
[3] J. Shim, K.A. Striebel, E.J. Cairns, J. Electrochem. Soc. 149 (2002) A1321–A1325.
[4] D.M. armorstein, T.H. Yu, K.A. Striebel, F.R. McLarnon, J. Hou, E.J. Cairns, J. Power Sources 89 (2000) 219–226.
[5] J. Nelson, S. Misra, Y. Yang, A. Jackson, Y.J. Liu, H.L. Wang, H.J. Dai, J.C. Andrews, Y. Cui, M.F. Toney, J. Am. Chem. Soc. 134 (2012) 6337–6343.
[6] S. Thieme, J. Brückner, I. Bauer, M. Oschatz, L. Borchardt, H. Althues, S. Kaskel, J. Mater. Chem. A 1 (2013) 9225–9234.
[7] S.R. Chen, Y.P. Zhai, G.L. Xu, Y.X. Jiang, D.Y. Zhao, J.T. Li, L. Huang, S.G. Sun, Electrochim. Acta 56 (2011) 9549–9555.
[8] J. Schuster, G. He, B. Mandlmeier, T. Yim, K.T. Lee, T. Bein, L.F. Nazar, Angew. Chem. Int. Ed. 51 (2012) 3591–3595.
[9] G.M. Zhou, D.W. Wang, F. Li, P.X. Hou, L.C. Yin, C. Liu, G.Q. Lu, I.R. Gentle, H.M. Cheng, Energy Environ. Sci. 5 (2012) 8901–8906.
[10] J.C. Guo, Y.H. Xu, C.S. Wang, Nano Lett. 11 (2011) 4288–4294.
[11] N. Jayaprakash, J. Shen, S.S. Moganty, A. Corona, L.A. Archer, Angew. Chem. Int. Ed. 50 (2011) 5904–5908.
[12] G.Y. Zheng, Y. Yang, J.J. Cha, S.S. Hong, Y. Cui, Nano Lett. 11 (2011) 4462–4467.
[13] H. Kim, H.D. Lim, J. Kim, K. Kang, J. Mater. Chem. A (2013), http://dx.doi.org/10.1039/C3TA12522J.
[14] J.Z. Wang, L. Lu, M. Choucair, J.A. Stride, X. Xu, H.K. Liu, J. Power Sources 196 (2011) 7030–7034.
[15] H.L. Wang, Y. Yang, Y.Y. Liang, J.T. Robinson, Y.G. Li, A. Jackson, Y. Cui, H.J. Dai, Nano Lett. 11 (2011) 2644–2647.
[16] F.F. Zhang, X.B. Zhang, Y.H. Dong, L.M. Wang, J. Mater. Chem. 22 (2012) 11452–11454.
[17] S. Evers, L.F. Nazar, Chem. Commun. 48 (2012) 1233–1235.
[18] N. Li, M. Zheng, H. Lu, Z. Hu, C. Shen, X. Chang, G. Ji, J. Cao, Y. Shi, Chem. Commun. 48 (2012) 4106–4108.
[19] L.Q. Lu, L.J. Lu, Y. Wang, J. Mater. Chem. A 1 (2013) 9173–9181.
[20] Y. Cao, X. Li, I.A. Aksay, J. Lemmon, Z. Nie, Z. Yang, J. Liu, Phys. Chem. Chem. Phys. 13 (2011) 7660–7665.
[21] B. Ding, C.Z. Yuan, L.F. Shen, G.Y. Xu, P. Nie, Q.X. Lai, G.X. Zhang, J. Mater. Chem. A 1 (2013) 1096–1101.
[22] L.W. Ji, M.M. Rao, H.M. Zheng, L. Zhang, Y.C. Li, W.H. Duan, J.H. Guo, E.J. Cairns, Y.G. Zhang, J. Am. Chem. Soc. 133 (2011) 18522–18525.
[23] C.X. Zu, A. Manthiram, Adv. Energy Mater. 8 (2013) 1008–1012.
[24] H.B. Wang, C.J. Zhang, Z.H. Liu, L. Wang, P.X. Han, H.X. Xu, K.J. Zhang, S.M. Dong, J.H. Yao, G.L. Cui, J. Mater. Chem. 21 (2011) 5430–5434.
[25] J.W. Lee, J.M. Ko, J.D. Kim, Electrochim. Acta 85 (2011) 459–466.
[26] G. Wu, N.H. Mack, W. Gao, S.G. Ma, R.Q. Zhong, J.T. Han, J.K. Baldwin, P. Zelenay, ACS Nano 11 (2012) 9764–9776.
[27] X.G. Sun, X.Q. Wang, R.T. Mayes, S. Dai, ChemSusChem 5 (2012) 2079–2085.
[28] F.G. Sun, J.T. Wang, H.C. Chen, W.C. Li, W.M. Qiao, D.H. Long, L.C. Ling, ACS Appl. Mater. Interfaces 12 (2013) 5630–5638.
[29] Z.G. Wang, X.Y. Niu, J. Xiao, C.M. Wang, J. Liu, F. Gao, RSC Adv. 3 (2013) 16775–16780.
[30] W.S. Hummers, R.E. Offman, J. Am. Chem. Soc. 80 (1958) 1339.
[31] L. Zhang, L. Ji, P.A. Glans, Y. Zhang, J. Zhu, J. Guo, Phys. Chem. Chem. Phys. 14 (2012) 13670–13675.
[32] V. Toniazzo, C. Mustin, J.M. Portal, B. Humbert, R. Benoit, R. Erre, Appl. Surf. Sci. 143 (1999) 229–237.
[33] F. Kapteijn, J.A. Moulijn, S. Matzner, H.P. Boehm, Carbon 37 (1999) 1143–1150.
[34] Y.X. Wang, L. Huang, L.C. Sun, S.Y. Xie, G.L. Xu, S.R. Chen, Y.F. Xu, J.T. Li, S.L. Chou, S.X. Dou, S.G. Sun, J. Mater. Chem. 22 (2012) 4744–4750.
[35] R.D. Rauh, K.M. Abraham, G.F. Pearson, J.K. Surprenant, S.B. Brummer, J. Electrochem. Soc. 126 (1979) 523–527.
[36] Y. Mao, H. Duan, B. Xu, L. Zhang, Y.S. Hu, C.C. Zhao, Z.X. Wang, L.Q. Chen, Y.S. Yang, Energy Environ. Sci. 5 (2012) 7950–7955.
[37] S.R. Narayanan, D.H. Shen, S. Surampudi, A.I. Attia, G. Halpert, J. Electrochem. Soc. 140 (1993) 1854–1861.